Subsurface Imaging of Soft Polymeric Materials with Nanoscale Resolution

Eike-Christian Spitzner,* Christian Riesch, and Robert Magerle*

Chemische Physik, Technische Universität Chemnitz, D-09107 Chemnitz, Germany

ARTICLE

ABSTRACT Nondestructive depth-resolved imaging of ~20-nm-thick surface layers of soft polymeric materials is demonstrated using amplitude modulation atomic force microscopy (AM-AFM). From a map of amplitude-phase-distance curves, the tip indentation into the specimen is determined. This serves as a depth coordinate for reconstructing cross sections and volume images of the specimen's mechanical properties. Our method reveals subsurface structures which are not discernible using conventional AM-AFM. Results for surfaces of a block copolymer and a semicrystalline polymer are presented.

KEYWORDS: surface properties · depth profiling · block copolymers · semicrystalline polymers · atomic force microscopy

The chemical composition and mechanical properties of the near-surface region of polymeric materials play a crucial role for understanding structure formation phenomena such as surface segregation,[1] wetting,[2] and surface reconstructions,[3] as well as adhesion[4] and friction.[5] Amplitude modulation atomic force microscopy (AM-AFM),[6,7] also known as tapping mode AFM, is a versatile and widely used method for imaging polymeric surfaces as well as other soft matter, including biological cells.[8,9] In AM-AFM, a cantilever with a sharp tip is excited to oscillate at (or near) its resonance frequency ω_0 and scanned along the surface of a specimen while keeping the oscillation amplitude A constant by adjusting the tip height using a feedback loop. These height changes reflect the shape of the sample surface. The simultaneously detected phase shift between the excitation signal and tip oscillation contains information about the local mechanical properties of the specimen. Compared to atomic force microscopy (AFM) in contact mode,[10] AM-AFM minimizes the lateral forces acting on the sample; however, the indentation of the tip into compliant specimens cannot be neglected. For instance, on flat but mechanically heterogeneous surfaces, the AM-AFM feedback loop varies the height of the tip to keep the amplitude A constant. Thus, the height images do not necessarily represent the true shape of the surface.[11] Furthermore, the phase images also include information from a certain volume below the surface due to tip indentation.[12]

In this article, we demonstrate a method which takes advantage of finite tip indentation to reconstruct depth-resolved images of material properties. The method is nondestructive, offers subnanometer depth resolution, and complements other AFM-based volume imaging techniques that use ablation,[13] ultrasonic excitation of the sample,[14,15] or require certain assumptions about the specimen.[16] Our approach relies on measurements of amplitude−phase−distance (APD) curves, where amplitude and phase are recorded as the tip−sample distance d is decreased. Knoll *et al.* used two-dimensional arrays of APD curves to determine the location of the true sample surface as given by the tip height h_0 where attractive forces first cause a phase change.[12] From this point on, the tip indentation $\tilde{z}$ can be determined by comparing the damped amplitude on the specimen with the damped amplitude on a noncompliant stiff surface.[12,17] APD curves have also been used to describe and identify tip−sample interaction processes, such as energy dissipation,[18−20] and different contributions to the origins of phase contrast.[21] By plotting the energy dissipated per oscillation cycle E_{dis} as a function of the amplitude set point ratio A/A_0 (where A_0 is the amplitude at a large tip−sample distance d), Garcia *et al.*[19] identified different dissipation processes corresponding to different types of tip−sample interaction. Schröter *et al.*[21] introduced a simple model which

*Address correspondence to eike-christian.spitzner@physik.tu-chemnitz.de, robert.magerle@physik.tu-chemnitz.de.

Received for review October 12, 2010 and accepted December 07, 2010.

Published online December 21, 2010.
10.1021/nn1027278

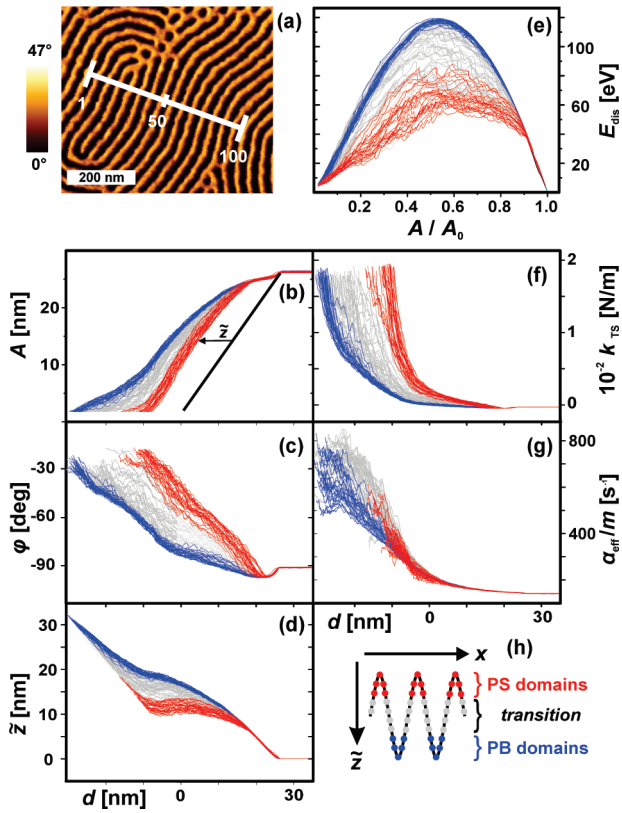

Figure 1. (a) AM-AFM phase image of the surface of an SB film ($A/A_0 = 0.77$). Bright (dark) areas correspond to PS (PB) microdomains below a PB top layer. The white line indicates the positions where $A(d)$ and $\varphi(d)$ (shown in panels b and d, respectively) have been measured. The solid line in panel b shows the expected amplitude on a nondeformable surface. The curves are colored according to position (PS domains, PB domains, transition regions) as indicated in panel h. (d) Tip indentation $\tilde{z}(d)$, (e) $E_{dis}(A/A_0)$, (f) $k_{TS}(d)$, and (g) $\alpha_{eff}/m(d)$ computed from APD data. (h) Schematic tip indentation $\tilde{z}$ as a function of position x for $A/A_0 \approx 0.5$ and region classification scheme according to tip indentation.

separates the conservative and dissipative contributions to tip−sample interaction, permitting a better understanding of image contrast formation.

RESULTS AND DISCUSSION

Our subsurface imaging method combines information about material properties, contrast formation in phase images, and uses the tip indentation as a depth coordinate. This is accomplished by measuring two-dimensional arrays of APD curves, where each curve contains information about the position of the true sample surface and the tip indentation, as well as depth-resolved information about the tip−sample interaction. The data analysis is described in the Materials and Methods section. We demonstrate this method on two polymeric model systems exhibiting nm-scale heterogeneities in the subsurface region. Both systems provide good contrast in AM−AFM phase imaging due to large differences in the mechanical properties of their respective components.

The first system is a thin film of polystyrene-*block*-polybutadiene (SB), which forms polystyrene (PS) cylinders embedded in a polybutadiene (PB) matrix[22,23] (Figure 1a). We recorded 100 APD curves separated by 5 nm along the line perpendicular to the PS cylinders as indicated in Figure 1a. In Figure 1b,c, the amplitude A and phase φ are plotted as a function of tip−sample distance d. Plotting the tip indentation $\tilde{z}$ *versus* d shows identical slopes for all indentation curves up to $d = 15$ nm (Figure 1d). This point corresponds to an indentation of 10 nm, the depth where the tip first touches the glassy (hard) PS cylinders, pushing through the compliant (soft) PB matrix. This is in agreement with earlier results.[12] In Figure 1e, the energy dissipated between the AFM tip and the sample per oscillation cycle, E_{dis}, is plotted as a function of the set point ratio A/A_0. Notably, all curves are congruent down to $A/A_0 = 0.91$. This reflects the presence of a 10-nm-thick top layer of PB. E_{dis} curves recorded on PS domains exhibit significantly different shapes and lower maximum values than those recorded on PB domains. We attribute the shape of the PB curves to viscoelastic dissipation processes[19] and note the plateau-like shape of the PS curves, similar to those curves observed on crystalline regions of polypropylene.[24] Figure 1 panels f and g show the analysis of the APD curves according to ref 21. Conservative and dissipative contributions to the total tip−sample interaction force are expressed by an additional tip−sample spring constant k_{TS} and the effective damping parameter α_{eff}/m. For k_{TS} as well as for A and φ, the curves recorded on PS and PB domains can be clearly distinguished. They split as d decreases, whereas for $d > A_0$, where tip−sample interactions are negligible, the curves attain the same value. The set of α_{eff}/m curves measured on PS domains can be identified by their lower maximum values (Figure 1f). Otherwise, the α_{eff}/m curves measured on different domains exhibit the same shape. The quantities shown demonstrate a clear contrast between the two components of the SB film and deliver quantitative information about the tip−sample interaction.

We now combine the knowledge about tip indentation $\tilde{z}$ for all tip−sample distances d (and the corresponding amplitude set points A/A_0) with the quantities describing the tip−sample interaction (φ, E_{dis}, k_{TS}, and α_{eff}/m) to create a depth-resolved image of the specimen. This requires no *a priori* information about the sample. In Figure 2, we plot φ, E_{dis}, k_{TS}, and α_{eff}/m as functions of lateral position x and depth z beneath the sample surface. Since surface roughness was not considerable, we set $z \equiv \tilde{z}$. The resulting depth-resolved data shown in Figure 2 correspond to cross sections through the SB film. Panel a is a plot of $\varphi(x, z)$ containing data from all APD curves, where the z axis has been stretched by a factor of 2.5. The black regions indicate areas where the given depth (tip indentation) was not reached. The phase shift shows periodic variations in the local mechanical properties, corresponding to the

regular spacing of PS cylinders. For detailed discussion, we selected two cylinders and plotted the aforementioned quantities on a magnified 1:1 scale (Figure 2b−e). In panel b, the phase shift $\varphi(x, z)$ gives a good impression of the general shape of the cylinders' surface, as expected from the AM-AFM phase image, and shows a monotonous slope starting at $z \simeq 5$ nm. The white lines indicate the tip indentation $\tilde{z}$ for the amplitude set points $A/A_0 = 0.999$, 0.95, 0.90 (light tapping), and 0.80 (moderate tapping). These lines correspond to the lower tip inflection point when imaging with conventional AM-AFM. The phase values along one line would result in one line of the AM-AFM phase image. For several common A/A_0 values, the tip inflection point visibly follows areas of nearly constant phase shift. This might partially explain the often poor phase contrast observed in AM-AFM imaging and its strong dependency on the amplitude set point A/A_0.[25] $E_{dis}(x, z)$ is plotted in panel c. Notably, most of the energy is dissipated in the soft matrix at positions between the PS cylinders at a depth of ~15 nm. Generally, E_{dis} attains lower values above stiff objects, which leads to weak but visible lateral contrast at depths of only 2−3 nm. The remaining two panels, d and e, show $k_{TS}(x, z)$ and $\alpha_{eff}/m(x, z)$. Both quantities exhibit almost constant values even for depths where $\varphi(x, z)$ has already notably increased. Furthermore, k_{TS} and α_{eff}/m grow with almost infinite slope close to the respective maximum tip indentation. Note that this drastic increase could not be completely resolved in panels d and e. To reconstruct a three-dimensional image from depth-resolved data, we use thresholding to obtain the isosurfaces of a given quantity, which separate stiffer objects from the surrounding matrix. Starting with the notion of circular cylinder cross sections, $\varphi(x, z)$ reflects the general shape but does not allow the location of the cylinder surfaces to be determined due to the continuous increase of the phase signal for $z > 5$ nm. E_{dis} is also not suitable for this purpose, leaving $k_{TS}(x, z)$ and $\alpha_{eff}/m(x, z)$. The cylinder surface is indicated by a strong increase in the two parameters mentioned above. In $k_{TS}(x, z)$, slight shadows appear above the cylinders. In $\alpha_{eff}/m(x, z)$, the cylinders appear broadened compared to $k_{TS}(x, z)$.

The second system is a thin film of elastomeric polypropylene.[26] Its surface properties and volume structure have been studied previously.[24,27−30] We investigated a 250 × 250 nm^2 surface area by recording 50 × 50 APD curves with 5-nm separation. From these data, we have reconstructed maps of k_{TS} as a function of depth z and combined them into a volume image. In Figure 3a, the k_{TS} isosurface is shown as yellow, enclosing the crystalline (hard) regions of ePP, whereas the amorphous (compliant) regions are shown as transparent. A cross section (x, z) along one lamella is presented

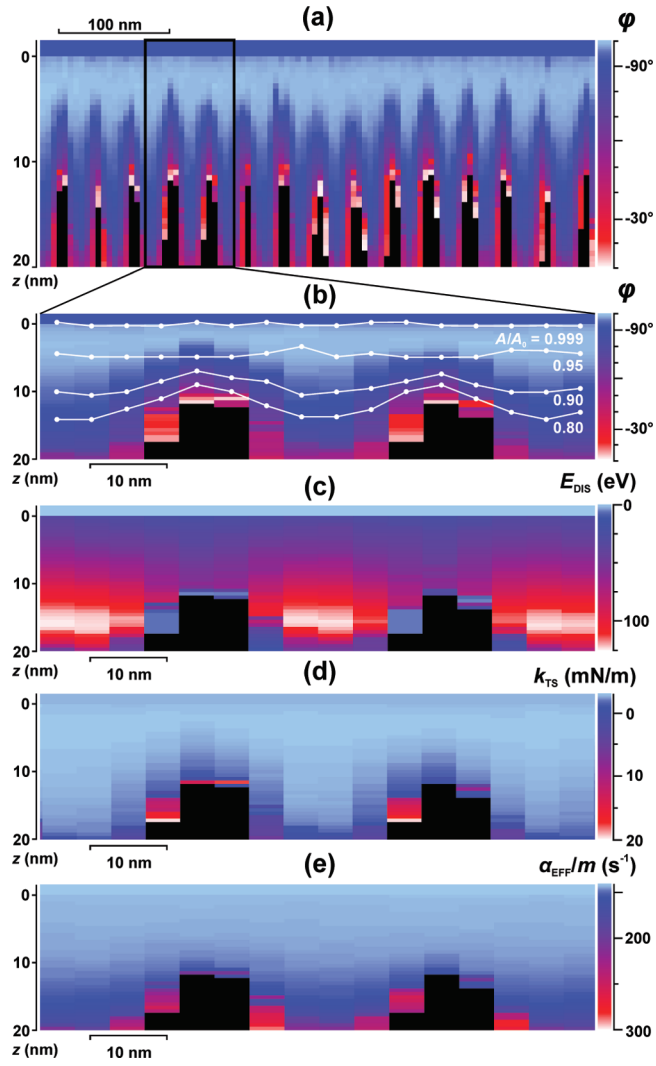

Figure 2. φ plotted as a function of depth z and position x along the white line shown in Figure 1a. (b−e) $\varphi(x, z)$, $E_{dis}(x, z)$, $k_{TS}(x, z)$, and $\alpha_{eff}/m(x, z)$ for the two indicated cylinders in 1:1 scaling. The white lines in panel b show the tip indentation $\tilde{z}$ for different set points A/A_0.

in Figure 3b. Figure 3c shows a conventional AM-AFM phase image of the area where the APD curves were measured. In Figure 3d,e, the k_{TS} slices for three different depths are presented. The gray scale has been adapted to the respective minimum and maximum. In contrast to the AM-AFM phase image, where only the lateral extension of lamellae is discernible, Figure 3 panels a and b show the detailed three-dimensional shape of the lamella edges. The latter display height corrugations of ~5 nm (in the z direction) and ~15-nm-large blocks along the lamellae, supporting earlier findings that crystalline lamellae are formed from grains of this size.[31] Furthermore, Figure 3b reveals the laterally heterogeneous thickness of the amorphous top layer as claimed in previous works.[24,32] This is corroborated by Figure 3d, where no crystalline regions are visible at a depth of $z = 1$ nm. In contrast, more and more lamellae appear at $z = 5$ and 15 nm (Figure 3 panels e and f,

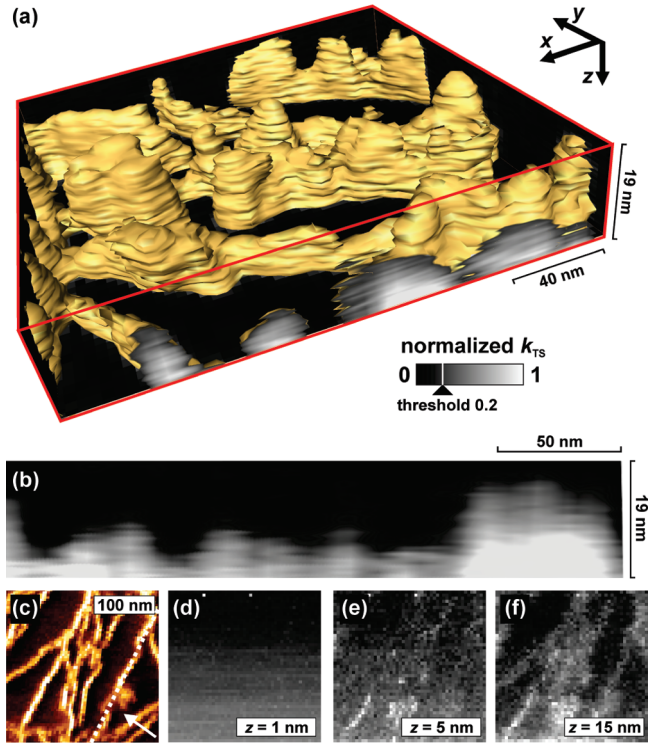

Figure 3. (a) Isosurface volume image reconstructed from normalized k_{TS} maps representing the top 19 nm of the ePP specimen. (b) Cross section through the volume image shown in panel a along one lamella marked with a dotted line in panel c. (c) AM-AFM phase image of the same spot ($A/A_0 = 0.90$). Crystalline lamellae appear bright, whereas dark regions indicate amorphous material. The viewing direction of the 3D volume image shown in panel a is indicated by a white arrow. (d–f) Normalized k_{TS} maps for 1, 5 nm, and 15 nm depth, respectively.

respectively). At larger depths, the lamellae appear broadened compared to those closer to the surface. This can be explained by the influence of the conical shape of the tip, which becomes greater with increasing z.

CONCLUSION

The method presented in this work allows objects located at the same depth which exhibit different mechanical properties to be distinguished from mechanically identical objects at different depths. In a conventional AM-AFM phase image, both would yield a similar signal. As a volume imaging technique, the lateral resolution is equal to that of AM-AFM and is mainly determined by the radius and shape of the tip. In contrast, the vertical resolution is only limited by the accuracy of the amplitude detection, which is ~0.5 nm in our case. Furthermore, while measuring APD curves, no lateral forces act on the sample and surface deformations due to tip indentation are reversible in most cases. The shape of hard objects embedded in a soft matrix can be reconstructed. However, no information is obtained from inside or below noncompliant objects. The depth range is limited by the tip indentation, which is primarily determined by the compliance of the material. For a given sample, the tip indentation can be increased by higher excitation amplitudes of the cantilever or by decreasing the lower limit of the amplitude in APD measurements. However, to avoid destruction of the specimen, a trade-off must be found.

The presented approach turns the finite tip indentation during AM-AFM imaging on soft specimens into an advantage. By analyzing maps of APD curves, we obtain the true sample surface, tip indentation, and depth resolved images of material properties in the subsurface region. This is achieved using standard AFM equipment and it opens a broad range of new research opportunities in nanoscience and soft matter physics, as well as biology, where the structure of the near surface region is of particular interest.

MATERIALS AND METHODS

Sample Preparation. Polystyrene-*block*-polybutadiene was obtained from Polymer Source, Inc., Canada, with weight averaged molecular weights $M_w^{PS} = 13.6$ kg · mol^{-1}, $M_w^{PB} = 33.7$ kg · mol^{-1} of the two blocks, and polydispersity $M_w/M_n = 1.03$. A 60-nm-thick film was prepared by spin-casting onto a silicon substrate from a 1 wt % solution in toluene, followed by annealing at 23 °C for 14 h in a nitrogen atmosphere with 70% partial pressure of chloroform vapor. This procedure results in polystyrene cylinders, which are aligned parallel to the surface and embedded in a polybutadiene matrix. Elastomeric polypropylene (ePP) with $M_w = 160$ kg · mol^{-1} and 36% crystallinity was synthesized using a dual-side metallocene catalyst as described in ref 26. A 240-nm-thick film was prepared by drop casting a 0.6 wt % decalin solution onto a silicon substrate. The sample was first heated to 150 °C in air to melt the polymer and then kept at 100 °C in a nitrogen atmosphere for 18 h to allow for slow crystallization. This leads to the formation of 15-nm-wide, crystalline lamellae surrounded by amorphous ePP.

Atomic Force Microscopy. All AFM measurements were accomplished using NanoWizard I and II devices (JPK Instruments AG, Berlin, Germany) under ambient conditions with silicon cantilevers (Pointprobe NCH, NanoWorld AG, Neuchâtel, Switzerland). The cantilever parameters were as follows: quality factor Q = 420, resonance frequency $\omega_0 = 248.904$ kHz, and spring constant $k = 16.5$ N/m (determined as in ref 33) for the measurements on SB. The excitation frequency $\omega = \omega_0$. For measurements on ePP, $Q = 435$, $\omega_0 = 287.939$ kHz, $k = 21.2$ N/m, and $\omega = 287.795$ kHz.

APD Curves. Amplitude A and phase φ were recorded pointwise by decreasing the tip height h. This is technically similar to the force volume technique, which is based on measuring static forces as a function of distance.[34−36] We measured APD curves at points separated by 5 nm along a line (in the case of SB) or a square grid (in the case of ePP).

Data Analysis. The APD curves have been analyzed according to the methods described in refs 12, 21, and 19. The unperturbed (true) sample surface $h_0(x, y)$ is the position where attractive forces first cause a phase change when approaching the surface by decreasing the AFM tip height h.[12] The tip−sample distance d is obtained by setting $d \equiv h - h_0 + A_0$. For plotting depth-resolved data, as shown in Figure 2, $h_0(x, y)$ measured from successively acquired curves must be consistent, which is hampered by thermal drift affecting the AFM components controlling the tip height. Standard methods, such as linewise subtraction of a best-fit first-order polynomial, are well-suited for correcting these drift effects. The tip indentation $\tilde{z} = A(d) - d$. In the case of considerable surface corrugation, slices with constant tip inden-

tation must be shifted by $h_0(x, y)$ to obtain a z coordinate with respect to the lab reference frame. In the case of our samples, surface roughness was not considerable (always <2.5 nm) and no lateral features appeared;[12,24] therefore we set $z \equiv \tilde{z}$. The energy dissipated between the AFM tip and the sample per oscillation cycle is given by[19]

$$E_{dis} = -\frac{\pi k A}{Q}\left(A_0 \sin\varphi + A\frac{\omega}{\omega_0}\right) \quad (1)$$

We use the phase convention of ref 21 where, in resonance, $\varphi = -90°$. Equation 1 has been adapted accordingly. Conservative and dissipative contributions to the total tip−sample interaction force are expressed by an additional tip−sample spring constant k_{TS} and the effective damping parameter α_{eff}/m.[21] The former is given by

$$k_{TS} = k_{eff} - k = m\left(\omega^2 + \cos(\varphi)\frac{F_0/m}{A}\right) - k \quad (2)$$

where $m = k/\omega_0^2$ is the vibrating mass and k_{eff} is the total effective spring constant. The effective damping parameter

$$\alpha_{eff}/m = \frac{-\sin(\varphi)}{\omega}\frac{F_0/m}{A} \quad (3)$$

The quantity F_0/m, where F_0 represents the amplitude of the excitation force, is obtained by fitting the cantilever resonance curve.[21]

In the case of ePP, we investigated a 250 × 250 nm^2 surface area by recording 50 × 50 APD curves with 5 nm separation. From these data, we have reconstructed maps of k_{TS} as a function of depth z, ranging from 1 to 20 nm in steps of 0.5 nm, resulting in 39 slices. To accentuate the lateral differences in k_{TS}, we subtracted each slice's background from the slice itself; the background was calculated by blurring with a 25-nm-wide Gaussian filter. The resulting slices were then combined into an isosurface volume image using Amira V4.0 (Mercury Computer Systems, Inc.).

Acknowledgment. We thank B. Rieger and A. Schöbel for providing the ePP, M. Neumann for sample preparation, and S. McGee for proofreading the manuscript. We acknowledge financial support from the Volkswagen Foundation.

REFERENCES AND NOTES

1. Puri, S. Surface-Directed Spinodal Decomposition. *J. Phys.: Condens. Matter* **2005**, *17*, R101.
2. Geoghegan, M.; Krausch, G. Wetting at Polymer Surfaces and Interfaces. *Prog. Polym. Sci.* **2003**, *28*, 261–302.
3. Rehse, N.; Knoll, A.; Konrad, M.; Magerle, R.; Krausch, G. Surface Reconstruction of an Ordered Fluid: An Analogy with Crystal Surfaces. *Phys. Rev. Lett.* **2001**, *87*, 035505.
4. Possart, W. *Adhesion: Current Research and Applications*; Wiley-VCH: Weinheim, Germany, 2005.
5. Persson, B. N. J. Sliding Friction. Surf. *Sci. Rep.* **1999**, *33*, 83–119.
6. Zhong, Q.; Inniss, D.; Kjoller, K.; Elings, V. Fractured Polymer/Silica Fiber Surface Studied by Tapping Mode Atomic Force Microscopy. *Surf. Sci.* **1993**, *290*, L688–L692.
7. García, R.; Pérez, R. Dynamic Atomic Force Microscopy Methods. *Surf. Sci. Rep.* **2002**, *47*, 197–301.
8. Magonov, S. N.; Whangbo, M.-H. *Surface Analysis with STM and AFM*; VCH: Weinheim, Germany, 1996.
9. Tsukruk, V. V., Ed. *Advances in Scanning Probe Microscopy of Polymers*; Macromolecular Symposia, Vol. 167; Wiley-VCH: Weinheim, Germany, 2001.
10. Binnig, G.; Quate, C. F.; Gerber, C. Atomic Force Microscope. *Phys. Rev. Lett.* **1986**, *56*, 930–933.
11. Brandsch, R.; Bar, G.; Whangbo, M.-H. On the Factors Affecting the Contrast of Height and Phase Images in Tapping Mode Atomic Force Microscopy. *Langmuir* **1997**, *13*, 6349–6353.
12. Knoll, A.; Magerle, R.; Krausch, G. Tapping Mode Atomic Force Microscopy on Polymers: Where Is the True Sample Surface? *Macromolecules* **2001**, *34*, 4159–4165.
13. Magerle, R. Nanotomography. *Phys. Rev. Lett.* **2000**, *85*, 2749–2752.
14. Shekhawat, G. S.; Dravid, V. P. Nanoscale Imaging of Buried Structures *via* Scanning Near-Field Ultrasound Holography. *Science* **2005**, *310*, 89–92.
15. Tetard, L.; Passian, A.; Thundat, T. New Modes for Subsurface Atomic Force Microscopy through Nanomechanical Coupling. *Nat. Nanotechnol.* **2010**, *5*, 105–109.
16. Bodiguel, H.; Montes, H.; Fretigny, C. Depth Sensing and Dissipation in Tapping Mode Atomic Force Microscopy. *Rev. Sci. Instrum.* **2004**, *75*, 2529–2535.
17. Höper, R.; Gesang, T.; Possart, W.; Hennemann, O.-D.; Boseck, S. Imaging Elastic Sample Properties with an Atomic Force Microscope Operating in the Tapping Mode. *Ultramicroscopy* **1995**, *60*, 17–24.
18. Hölscher, H. Quantitative Measurement of Tip−Sample Interactions in Amplitude Modulation Atomic Force Microscopy. *Appl. Phys. Lett.* **2006**, *89*, 123109.
19. García, R.; Gómez, C. J.; Martinez, N. F.; Patil, S.; Dietz, C.; Magerle, R. Identification of Nanoscale Dissipation Processes by Dynamic Atomic Force Microscopy. *Phys. Rev. Lett.* **2006**, *97*, 016103.
20. Cleveland, J. P.; Anczykowski, B.; Schmid, A. E.; Elings, V. B. Energy Dissipation in Tapping-Mode Atomic Force Microscopy. *Appl. Phys. Lett.* **1998**, *72*, 2613–2615.
21. Schröter, K.; Petzold, A.; Henze, T.; Thurn-Albrecht, T. Quantitative Analysis of Scanning Force Microscopy Data Using Harmonic Models. *Macromolecules* **2009**, *42*, 1114–1124.
22. Knoll, A.; Horvat, A.; Lyakhova, K. S.; Krausch, G.; Sevink, G. J. A.; Zvelindovsky, A. V.; Magerle, R. Phase Behavior in Thin Films of Cylinder-Forming Block Copolymers. *Phys. Rev. Lett.* **2002**, *89*, 035501.
23. Tsarkova, L.; Knoll, A.; Krausch, G.; Magerle, R. Substrate-Induced Phase Transitions in Thin Films of Cylinder-Forming Diblock Copolymer Melts. *Macromolecules* **2006**, *39*, 3608–3615.
24. Dietz, C.; Zerson, M.; Riesch, C.; Franke, M.; Magerle, R. Surface Properties of Elastomeric Polypropylenes Studied with Atomic Force Microscopy. *Macromolecules* **2008**, *41*, 9259–9266.
25. Magonov, S.; Elings, V.; Whangbo, M.-H. Phase Imaging and Stiffness in Tapping-Mode Atomic Force Microscopy. *Surf. Sci.* **1997**, *375*, L385–L391.
26. Dietrich, U.; Hackmann, M.; Rieger, B.; Klinga, M.; Leskelä, M. Control of Stereoerror Formation with High-Activity "Dual-Side" Zirconocene Catalysts: A Novel Strategy To Design the Properties of Thermoplastic Elastic Polypropenes. *J. Am. Chem. Soc.* **1999**, *121*, 4348–4355.
27. Karger-Kocsis, J. *Polypropylene: Structure, Blends and Composites*; Chapman & Hall: London, 1995; *Vol. 1*.
28. Rehse, N.; Marr, S.; Scherdel, S.; Magerle, R. Three-Dimensional Imaging of Semicrystalline Polypropylene with 10 nm Resolution. *Adv. Mater.* **2005**, *17*, 2203–2206.
29. Franke, M.; Rehse, N. Three-Dimensional Structure Formation of Polypropylene Revealed by *in Situ* Scanning Force Microscopy and Nanotomography. *Macromolecules* **2008**, *41*, 163–166.
30. Franke, M.; Rehse, N. Nucleation of Branches in Elastomeric Polypropylene. *Polymer* **2008**, *49*, 4328–4331.
31. Hugel, T.; Strobl, G.; Thomann, R. Building Lamellae from Blocks: The Pathway Followed in the Formation of Crystallites of Syndiotactic Polypropylene. *Acta Polym.* **1999**, *50*, 214–217.
32. Sakai, A.; Tanaka, K.; Fujii, Y.; Nagamura, T.; Kajiyama, T. Structure and Thermal Molecular Motion at Surface of Semi-Crystalline Isotactic Polypropylene Films. *Polymer* **2005**, *46*, 429–437.

33. Sader, J. E.; Chon, J. W. M.; Mulvaney, P. Calibration of Rectangular Atomic Force Microscope Cantilevers. *Rev. Sci. Instrum.* **1999**, *70*, 3967–3969.
34. Rotsch, C.; Radmacher, M. Mapping Local Electrostatic Forces with the Atomic Force Microscope. *Langmuir* **1997**, *13*, 2825–2832.
35. A-Hassan, E.; Heinz, W. F.; Antonik, M. D.; D'Costa, N. P.; Nageswaran, S.; Schoenenberger, C.-A.; Hoh, J. H. Relative Microelastic Mapping of Living Cells by Atomic Force Microscopy. *Biophys. J.* **1998**, *74*, 1564–1578.
36. Heinz, W. F.; Hoh, J. H. Spatially Resolved Force Spectroscopy of Biological Surfaces Using the Atomic Force Microscope. *Trends Biotechnol.* **1999**, *17*, 143–150.